Mechanisms governing the settling velocities and spatial distributions of inertial particles in wall-bounded turbulence

A. D. Bragg, D. H. Richter, and G. Wang

Mechanisms governing the settling velocities and spatial distributions of inertial particles in wall-bounded turbulence

A.D. Bragg[*]

Department of Civil and Environmental Engineering,

Duke University, Durham, NC 27708, USA

D. H. Richter

Department of Civil and Environmental Engineering and Earth Sciences,

University of Notre Dame, Notre Dame, IN 46556, USA

G. Wang[†]

Physics of Fluids Group and Twente Max Planck Center,

Department of Science and Technology, Mesa+ Institute,

and J. M. Burgers Center for Fluid Dynamics, University of Twente,

P.O. Box 217, 7500 AE Enschede, The Netherlands

(Dated: May 20, 2021)

Abstract

We use theory and Direct Numerical Simulations (DNS) coupled with point-particles to explore the average vertical velocities and spatial distributions of inertial particles settling in a wall-bounded turbulent flow. The theory is based on the exact phase-space equation for the Probability Density Function describing particle positions and velocities. This allows us to identify the distinct physical mechanisms governing the particle transport, which we then examine using the DNS data, and relate them to the well-known preferential sweeping mechanism in homogeneous isotropic turbulence. When the average vertical particle mass flux is zero, the averaged vertical particle velocity is zero away from the wall due to the particles preferentially sampling regions where the fluid velocity is positive, which balances with the downward Stokes settling velocity. When the average mass flux is negative, the combined effects of turbulence and particle inertia lead to average vertical particle velocities that can significantly exceed the Stokes settling velocity, by as much as ten times. Sufficiently far from the wall, the enhanced vertical velocities are due to the preferential sweeping mechanism. However, as the particles approach the wall, the contribution from the preferential sweeping mechanism becomes small, and a downward contribution from the turbophoretic velocity dominates the behavior. Close to the wall, the particle concentration grows dramatically, and the behavior is directly related to the behavior of the mechanisms governing the particle settling velocity. Finally, our results highlight how the Rouse model of particle concentration is to be modified for particles with finite inertia, by identifying particular mechanisms missing from that model due to its assumption of vanishing inertia.

I. INTRODUCTION

It is well-known that in homogeneous, isotropic turbulence (HIT), small particles with non-negligible inertia will settle at a rate that can exceed their Stokes settling velocity. Maxey [1] and Wang and Maxey [2] were among the first to outline and characterize the so-called preferential sweeping mechanism, according to which particles falling under the influence of gravity are swept around the downward side of eddies in HIT. This biased sampling of the background velocity field often leads to an average downwards particle velocity that is larger than that if the particles were settling in a quiescent medium — an effect which has been seen in direct numerical simulation (DNS) [2, 3] and experiments [4–7]. It has even been observed in the settling of snowflakes through the atmospheric boundary layer [8].

Accordingly, much effort has been directed at understanding the nature of this effect. It is generally accepted that the maximum observed modification to the settling velocity occurs at a Stokes number (based on the Kolmogorov scales) of order unity, and parameterizations have

* andrew.bragg@duke.edu
† g.wang@utwente.nl

been developed to describe this [9]. However, there are still questions regarding the magnitude of this effect, as well as how this magnitude depends on other nondimensional parameters such as the Froude number or Reynolds number. The work of Good *et al.* [10] nicely maps out the various settling regimes, and also addresses the possibility of turbulence retarding the settling velocity of inertial particles and how this relates to the drag law in DNS laden with point particles. Furthermore, the recent study of Tom and Bragg [11] advanced the work of Maxey [1] by developing a theoretical framework that is valid for arbitrary particle inertia and reveals the contribution that different turbulent scales make to the enhanced settling, and how this depends on Stokes number, Froude number, and flow Reynolds number. The theory predicts that for particles with finite inertia, the Reynolds number dependence will always saturate, and that the saturation Reynolds number is a non-decreasing function of particle inertia. These predictions were confirmed by DNS results.

While all of the aforementioned studies have focused on HIT, the picture is significantly less clear in the context of wall-bounded turbulent flows. Much work has been aimed at understanding the interaction of coherent structures with inertial particles, including transport to/from the wall [12, 13], and the turbophoretic drift [14–16]; however, the vast majority of these studies neglect wall-normal gravity. Indeed, discrepancies in certain particle velocity statistics between experimental setups with horizontal [17–19] versus vertical [20, 21] channels are possibly due to differences in gravitational orientation. The recent DNS of Lee and Lee [22] demonstrates that for two-way coupled flows, the addition of wall-normal gravity can even qualitatively alter the interaction between inertial particles and near-wall streaks and coherent structures via mechanisms similar to that of Wang and Maxey [2].

Generally speaking, the question of inertial particle settling through wall-bounded turbulence has been largely avoided, and is complicated by several factors as compared to HIT. First, the process of turbophoresis, which is absent in HIT due to a lack of mean gradient in turbulence kinetic energy, is difficult to distinguish from the preferential sweeping mechanism, although they are distinct phenomena. Secondly, the smallest time scales of the flow actually vary with wall-normal location, so it should not be expected that the settling rate is simply a function only of a single Stokes number. The velocity of a particle falling through a flow with spatially varying time scales would be a function of wall-normal distance, and will be influenced by the flow Reynolds number as well. Third, rigorous phase-space probability density function theories of particle transport in inhomogeneous turbulence suggest that there is an additional drift effect that contributes to the wall-normal particle motion, which arises from the inhomogeneity but is distinct from the

turbophoretic drift, and exists even in the absence of gravitational settling [23–26]. The importance of this additional drift compared with the gravitational and turbophoretic drifts is not well understood, and it is difficult to develop closed expressions that capture its influence [27]. It is one of the goals of this work to distinguish between these transport mechanisms and determine their relative importance.

The settling velocity of inertial particles in wall-bounded flows is also important because it controls the spatial distribution of the particles. In an effort to theoretically extend the logarithmic profile of wall turbulence for passive scalars, Rouse [28] derived the well-known power law for the average concentration when the scalar experiences gravitational settling towards the wall, where the power is proportional to the Stokes settling velocity of the particle. This theory, which is valid only within the logarithmic region of the turbulent boundary layer, assumes that gravitational settling is balanced by turbulent fluxes on average, so the net flux is zero at any height and the magnitude of the downward settling flux is equal to the upward turbulent flux. This so-called flux-profile relationship between the mean concentration and flux is the basis for many geophysical measurements which attempt to estimate the surface emission of discrete particles like snow, dust, or water droplets [29–31], as well as for determining how to specify boundary conditions for heavy particles in coarse-scale numerical models [32]. Since then, further modifications to the theory of Rouse [28] have been made, such as incorporating a net imbalance between the gravitational and turbulent fluxes [30, 33]. Freire *et al.* [34] extended the theory to non-neutral stability, including the effects of both stable and unstable stratification, while Nissanka *et al.* [35] considered the full boundary layer (i.e. not restricted only to the surface layer). Other studies, such as those by Pan *et al.* [36] and Zhu *et al.* [37], explore beyond the one-dimensional framework by incorporating a streamwise dependence in addition to height.

In addition to these, it is also becoming clear that particle inertia causes deviations from the traditional Rouse theory. The recent experiments of Berk and Coletti [38] and Baker and Coletti [39] show clearly that particle inertia causes weaker gradients of wall-normal concentration as the Stokes number is increased, as compared to that predicted by Rouse theory. From a more theoretical perspective, Richter and Chamecki [40] attempted to incorporate inertial effects into the framework of Rouse [28] by using a first-order perturbation expansion of the particle advection velocity with Stokes number in the equation for mean particle concentration [1, 41, 42]. This inertial correction to the particle advection velocity provided concentration profiles that matched DNS results, but only in the limit of small Stokes numbers, as expected. For finite particle inertia, the underlying framework of Rouse [28] is called into question, because the equation ignores the

contributions from a number of different mechanisms that are crucial when the Stokes number is not small.

In this study, therefore, we set out to understand and quantify the relevant transport mechanisms for inertial particles settling through a wall-bounded turbulent flow, for the dilute, one-way coupled regime. This is done by examining the problem through a phase-space probability density formulation, where the magnitudes and regimes of relevance for the various distinct inertial effects are calculated via idealized point-particle DNS. The goal is to clarify the multiple pathways through which inertia can affect the flux-profile relationship in wall-bounded turbulence, in order to clear the way towards more theoretically sound extensions to the theory of Rouse [28] in the future. Section II outlines the theoretical framework by casting the problem in phase space, and section III describes the DNS used to generate the data. We then discuss the results in section IV.

II. THEORY

We consider particles with particle-to-fluid density ratio $\rho_p/\rho_f \gg 1$, and whose size is smaller than the smallest length scales of the wall-bounded turbulence. Furthermore, we also consider mass and volume loadings such that the one-way coupled, dilute regime applies. In this case, the equations of motion are

$$d\bm{x}^p(t) = dt\bm{v}^p(t) + \sqrt{2\kappa dt}d\bm{\xi}(t), \tag{1}$$

$$\frac{d}{dt}\bm{v}^p(t) = \frac{\Psi}{\tau_p}\Big(\bm{U}^p(t) - \bm{v}^p(t)\Big) + \bm{g}, \tag{2}$$

where $\bm{x}^p(t), \bm{v}^p(t)$ are the particle position and velocity, τ_p is the particle response time, $\bm{U}^p(t) \equiv \bm{U}(\bm{x}^p(t), t)$ corresponds to the fluid velocity field evaluated at the particle position, κ is a constant diffusion coefficient, and $\bm{g}$ is gravity. The term $d\bm{\xi}(t)$ is a normalized vector-valued Wiener process with unit variance. This diffusion term is included since it will be used in the DNS in order to enable the particles to be suspended from the wall and generate a configuration where the vertical particle mass flux is zero. It is not meant to imply that the inertial particles experience molecular diffusion, but rather this term is simply used as a tool for one of the DNS arrangements described in more detail below. Its presence does not influence the main goals of the work since we will choose κ to be sufficiently small so that the related diffusion only affects the particle motion at distances less than one viscous wall unit from the wall. It is also helpful to include this term in the analysis since such a term was included in the model of Rouse [28]. This ensures that our transport equations reduce to those discussed in that work in the limits of vanishing particle inertia

and $\kappa \to \kappa_f$, where κ_f is the fluid mass diffusivity.

The variable $\Psi \equiv [1 + 0.15(Re_p)^{0.687}]$ appears due to using the Schiller-Naumann [43] hydrodynamic drag force model, where Re_p is the particle Reynolds number. In the theoretical developments below, for analytical tractability we assume $Re_p \to 0$ and hence take $\Psi = 1$. In the DNS this assumption will not be made, however, the DNS results show that on average $Re_p < 1$. As a result, the assumption that $\Psi = 1$ in the theory will only lead to minor differences between the theory and DNS.

Other forces acting on the particle in the near-wall region, such as lift forces [44], could also be important to account for. However, for the current work it is desirable to neglect such additional effects in order to focus on and understand the intricate role of the other mechanics at play in the system, such as those already captured in (2). Future work will extend the description to include further effects, such as lift forces, which can then be compared to the results from this present work to understand the role of these additional effects.

We consider the particle motion in a phase-space $\boldsymbol{x}, \boldsymbol{v}$ with Probability Density Function (PDF)

$$\mathcal{P}(\boldsymbol{x}, \boldsymbol{v}, t) \equiv \Big\langle \delta(\boldsymbol{x}^p(t) - \boldsymbol{x})\delta(\boldsymbol{v}^p(t) - \boldsymbol{v}) \Big\rangle, \tag{3}$$

that satisfies $\int_{\mathbb{R}^3} \int_\Omega \mathcal{P}(\boldsymbol{x}, \boldsymbol{v}, t)\, d\boldsymbol{x}\, d\boldsymbol{v} = 1$, where $\Omega \subset \mathbb{R}^3$ denotes the domain of the flow. Here, $\langle \cdot \rangle$ denotes an ensemble average over all realizations of the system, and $\delta()$ denotes a Dirac distribution. The exact PDE governing $\mathcal{P}$ is [45]

$$\begin{aligned}
\partial_t \mathcal{P} + \boldsymbol{v} \cdot \boldsymbol{\nabla}_{\boldsymbol{x}} \mathcal{P} = {}& \kappa \boldsymbol{\nabla}_{\boldsymbol{x}}^2 \mathcal{P} - \frac{1}{\tau_p} \boldsymbol{\nabla}_{\boldsymbol{v}} \cdot \Big(\langle \boldsymbol{U} \rangle \mathcal{P} \Big) \\
& - \frac{1}{\tau_p} \boldsymbol{\nabla}_{\boldsymbol{v}} \cdot \Big(\mathcal{P} \langle \boldsymbol{u}^p(t) \rangle_{\boldsymbol{x},\boldsymbol{v}} \Big) + \frac{1}{\tau_p} \boldsymbol{\nabla}_{\boldsymbol{v}} \cdot \Big(\boldsymbol{v} \mathcal{P} \Big) - \boldsymbol{g} \cdot \boldsymbol{\nabla}_{\boldsymbol{v}} \mathcal{P},
\end{aligned} \tag{4}$$

where $\boldsymbol{\nabla}_{\boldsymbol{x}}^2 = \boldsymbol{\nabla}_{\boldsymbol{x}} \cdot \boldsymbol{\nabla}_{\boldsymbol{x}}$, the operator $\langle \cdot \rangle_{\boldsymbol{x},\boldsymbol{v}}$ denotes an ensemble average conditioned on $\boldsymbol{x}^p(t) = \boldsymbol{x}$, $\boldsymbol{v}^p(t) = \boldsymbol{v}$, and $\boldsymbol{u}^p(t) \equiv \boldsymbol{u}(\boldsymbol{x}^p(t), t)$, where $\boldsymbol{u}(\boldsymbol{x}, t) \equiv \boldsymbol{U}(\boldsymbol{x}, t) - \langle \boldsymbol{U}(\boldsymbol{x}, t) \rangle$ is the fluctuating component of the fluid velocity field.

From (4), the transport equations governing the moments of the PDF may be constructed (see also [16, 46–48] for similar approaches to constructing the transport equations). The zeroth moment obeys the equation

$$\frac{D}{Dt}\varrho = -\varrho \boldsymbol{\nabla}_{\boldsymbol{x}} \cdot \langle \boldsymbol{v}^p(t) \rangle_{\boldsymbol{x}} + \kappa \boldsymbol{\nabla}_{\boldsymbol{x}}^2 \varrho, \tag{5}$$

where

$$\frac{D}{Dt} \equiv \partial_t + \langle \boldsymbol{v}^p(t) \rangle_{\boldsymbol{x}} \cdot \boldsymbol{\nabla}_{\boldsymbol{x}}, \tag{6}$$

6

the operator $\langle \cdot \rangle_{\boldsymbol{x}}$ denotes an ensemble average conditioned on $\boldsymbol{x}^p(t) = \boldsymbol{x}$, and

$$\varrho(\boldsymbol{x}, t) \equiv \int_{\mathbb{R}^3} \mathcal{P}(\boldsymbol{x}, \boldsymbol{v}, t) \, d\boldsymbol{v}, \tag{7}$$

is the marginal PDF that describes the spatial distribution of the particles.

The first moment describes the momentum of the particle phase and is governed by

$$\varrho \frac{D}{Dt} \langle \boldsymbol{v}^p(t) \rangle_{\boldsymbol{x}} = \kappa \boldsymbol{\nabla}_{\boldsymbol{x}}^2 \varrho \langle \boldsymbol{v}^p(t) \rangle_{\boldsymbol{x}} - \boldsymbol{\nabla}_{\boldsymbol{x}} \cdot \varrho \boldsymbol{S} + \frac{\varrho}{\tau_p} \langle \boldsymbol{u}^p(t) \rangle_{\boldsymbol{x}} + \frac{\varrho}{\tau_p} \langle \boldsymbol{U} \rangle - \frac{\varrho}{\tau_p} \langle \boldsymbol{v}^p(t) \rangle_{\boldsymbol{x}} + \varrho \boldsymbol{g}, \tag{8}$$

$$\boldsymbol{S}(\boldsymbol{x}, t) \equiv \left\langle \left(\boldsymbol{v}^p(t) - \langle \boldsymbol{v}^p(t) \rangle_{\boldsymbol{x}} \right) \left(\boldsymbol{v}^p(t) - \langle \boldsymbol{v}^p(t) \rangle_{\boldsymbol{x}} \right) \right\rangle_{\boldsymbol{x}}, \tag{9}$$

where $\boldsymbol{S}$ is the particle fluctuating velocity covariance tensor. We may also rearrange this equation as an expression for the mean particle velocity

$$\langle \boldsymbol{v}^p(t) \rangle_{\boldsymbol{x}} = -\tau_p \frac{D}{Dt} \langle \boldsymbol{v}^p(t) \rangle_{\boldsymbol{x}} + \frac{\tau_p \kappa}{\varrho} \boldsymbol{\nabla}_{\boldsymbol{x}}^2 \varrho \langle \boldsymbol{v}^p(t) \rangle_{\boldsymbol{x}} - \frac{\tau_p}{\varrho} \boldsymbol{\nabla}_{\boldsymbol{x}} \cdot \varrho \boldsymbol{S} + \langle \boldsymbol{u}^p(t) \rangle_{\boldsymbol{x}} + \langle \boldsymbol{U} \rangle + \tau_p \boldsymbol{g}. \tag{10}$$

Equations (5) and (10) for ϱ and $\langle \boldsymbol{v}^p(t) \rangle_{\boldsymbol{x}}$, respectively, are exact, and do not introduce any approximations beyond those already contained in the equations of motion (1) and (2) themselves.

A. Vertical transport in a stationary, wall-bounded turbulent flow

In this study we consider a horizontal, statistically stationary turbulent channel flow, and denote by $\boldsymbol{e}_z$ the unit vector in the vertical direction, with $\boldsymbol{g} = -g\boldsymbol{e}_z$, $\boldsymbol{x} \cdot \boldsymbol{e}_z = z$, $\boldsymbol{e}_z \cdot \boldsymbol{\nabla}_{\boldsymbol{x}} = \nabla_z$, $\boldsymbol{v}^p(t) \cdot \boldsymbol{e}_z = w^p(t)$, $\boldsymbol{u} \cdot \boldsymbol{e}_z = u$, $\langle \boldsymbol{U} \rangle \cdot \boldsymbol{e}_z = 0$. We then obtain from (5) and (10)

$$\varrho = (\Phi + \kappa \nabla_z \varrho) \langle w^p(t) \rangle_z, \tag{11}$$

$$\langle w^p(t) \rangle_z = \underbrace{-\frac{\tau_p}{2} \nabla_z \langle w^p(t) \rangle_z^2}_{\text{R1}} - \underbrace{\frac{\tau_p}{\varrho} S \nabla_z \varrho}_{\text{R2}} - \underbrace{\tau_p \nabla_z S}_{\text{R3}} + \underbrace{\langle u^p(t) \rangle_z}_{\text{R4}} - \underbrace{\tau_p g}_{\text{R5}} + \underbrace{\frac{\tau_p \kappa}{\varrho} \nabla_z^2 \varrho \langle w^p(t) \rangle_z}_{\text{R6}}, \tag{12}$$

where Φ is an integration constant that is determined by the boundary conditions and physically corresponds to the total net mass flux, and $S = \boldsymbol{S} : (\boldsymbol{e}_z \boldsymbol{e}_z)$. These equations are unclosed, both due to $\langle u^p(t) \rangle_z$ and S. Detailed physical interpretations of each term appearing in (12) will be given in subsequent sections.

Equation (11) is singularly perturbed with respect to κ, and therefore for $\kappa \neq 0$ the solution to (11) is

$$\varrho = \frac{\Phi}{\kappa} \int_0^z \mathcal{I}(z, y) \, dy, \tag{13}$$

$$\mathcal{I}(z, y) \equiv \exp \left(\frac{1}{\kappa} \int_y^z \langle w^p(t) \rangle_q \, dq \right), \tag{14}$$

while for $\kappa = 0$ we have simply $\varrho = \Phi/\langle w^p(t)\rangle_z$. In either case, this highlights that understanding $\langle w^p(t)\rangle_z$ is important not only to quantify the average settling velocity of the particles, but also because it determines the distribution $\varrho(z)$ for a given mass flux Φ.

We introduce the local Stokes number $St \equiv \tau_p/\tau_L$, where $\tau_L(z)$ is the fluid integral timescale at height z from the wall, and the Froude number $Fr \equiv \langle \|\boldsymbol{a}\|^2 \rangle^{1/2}/g$, where $\boldsymbol{a}$ is the fluid acceleration. In the limit $St \to 0$ with finite St/Fr, (12) reduces to $\langle w^p(t)\rangle_z = \langle u^p(t)\rangle_z - \tau_p g$. With this asymptotic behavior, then for the zero-flux case $\Phi = 0$, we obtain from (11)

$$0 = \varrho\langle u^p(t)\rangle_z - \tau_p \varrho g - \kappa \nabla_z \varrho. \tag{15}$$

Using a gradient-diffusion approximation $\varrho\langle u^p(t)\rangle_z \approx -\mathcal{K}\nabla_z \varrho$ leads to

$$0 = -(\mathcal{K} + \kappa)\nabla_z \varrho - \tau_p \varrho g. \tag{16}$$

The result in (16) corresponds to the phenomenological model for ϱ by Rouse [28] when the diffusion coefficient $\mathcal{K}$ is based on an eddy-diffusivity approximation for the log-law region of a wall-bounded turbulent flow. As the analysis above shows, (16) is restricted to the limit $St \to 0$ with St/Fr finite, and an important challenge is how the Rouse model is to be extended to capture the effects of finite particle inertia, as attempted in Richter and Chamecki [40]. Moreover, there is uncertainty regarding the validity of the gradient-diffusion closure $\varrho\langle u^p(t)\rangle_z \approx -\mathcal{K}\nabla_z \varrho$. One purpose of this paper is to carefully analyze how the model of [28] should be extended to more general cases, and the implications of the gradient-diffusion closure $\varrho\langle u^p(t)\rangle_z \approx -\mathcal{K}\nabla_z \varrho$. The other purpose is to consider the mechanisms governing $\langle w^p(t)\rangle_z$, which have been theoretically analyzed for HIT flows (e.g. [1, 11]), but have not been considered in detail for wall-bounded turbulent flows.

The equations governing ϱ for arbitrary St and Fr are given by (11) and (12). Therefore, to understand and model the more general case, we must understand the role played by each term that appears in these equations. We will consider this, first by considering their behavior in the quasi-homogeneous regions in the outer layer, and then close to the wall where the flow is strongly inhomogeneous.

B. Quasi-homogeneous region

In the quasi-homogeneous region away from the wall, the concentration profile is approximately constant ($\nabla_z \varrho \approx 0$) and from (11) and (12) we obtain

$$\varrho\langle w^p(t)\rangle_z = \Phi \approx \varrho\langle u^p(t)\rangle_z - \tau_p \varrho g, \tag{17}$$

where $\langle u^p(t)\rangle_z$ is constant. In this regime, the mean particle momentum is governed by the Stokes terminal velocity $\tau_p g$ and a contribution from the average fluid velocity sampled by the particles (commonly also called the "fluid seen by the particle"), namely $\langle u^p(t)\rangle_z$.

We may write

$$\varrho\langle u^p(t)\rangle_z = \varrho\langle u^p(t)\rangle_{\boldsymbol{x}} = \langle u(\boldsymbol{x},t)\delta(\boldsymbol{x}^p(t) - \boldsymbol{x})\rangle, \tag{18}$$

where $\boldsymbol{x}^p(t) \cdot \boldsymbol{e}_z = z^p(t)$, $u(\boldsymbol{x},t) \equiv \boldsymbol{e}_z \cdot \boldsymbol{u}(\boldsymbol{x},t)$, and the first equality holds because the flow is homogeneous in the horizontal directions. For particles that are (instantaneously) uniformly distributed in space, $\delta(\boldsymbol{x}^p(t)-\boldsymbol{x})$ is constant, and so $\langle u(\boldsymbol{x},t)\delta(\boldsymbol{x}^p(t)-\boldsymbol{x})\rangle = \langle u(\boldsymbol{x},t)\rangle\delta(\boldsymbol{x}^p(t)-\boldsymbol{x}) = 0$. If the particles are non-uniform in space, $\langle u(\boldsymbol{x},t)\delta(\boldsymbol{x}^p(t)-\boldsymbol{x})\rangle$ may be finite if there is a correlation between $u(\boldsymbol{x},t)$ and $\boldsymbol{x}^p(t)$ [25].

For the case where $\Phi < 0$, Maxey [1] argued that the particles are preferentially swept around the downward moving side of vortices in the flow where $u < 0$, leading to $\langle u^p(t)\rangle_z < 0$. As a result, turbulence enhances the settling velocity of the particles compared to the Stokes settling velocity $\tau_p g$. In the regimes $St \ll 1$ and $St \gg 1$, $\langle u^p(t)\rangle_z = 0$ because the particles are uniformly dstributed in these regimes. In the regime of rapidly settling particles, i.e. $Sv \equiv \tau_p g/\sqrt{\langle uu\rangle} \gg 1$, the correlation timescale of $u^p(t)$ vanishes [49, 50] and as a result $\langle u^p(t)\rangle_z = 0$ since there is no correlation between the particle motion and the local value of $u^p(t)$ in this limit. Similarly, in the regime $Sv \ll 1$, $\langle u^p(t)\rangle_z = 0$ because the symmetry breaking effect of gravity that generates preferential sweeping vanishes in this regime.

For the case where $\Phi = 0$, then we must have $\langle u^p(t)\rangle_z = \tau_p g$. In this regime, the finitude of $\langle u^p(t)\rangle_z$ is due to the fact that in order for the vertical flux to be zero, the particles must preferentially sample upward moving regions of the fluid velocity field. Therefore, although particles moving down towards the wall may still experience the preferential sweeping mechanism that causes them to preferentially sample downward moving fluid, this contribution is overwhelmed by the contribution of particles moving up which necessarily experience strongly positive regions of the flow in order to satisfy $\Phi = 0$.

In view of these considerations, we see that even for homogeneous flows, the importance of the preferential sweeping mechanism depends upon the boundary conditions in the system that determine the flux $\varrho\langle w^p(t)\rangle_z = \Phi$; this will be seen below to guide two different configurations of

the DNS. The presence of the wall provides a way for the zero-flux scenario $\Phi = 0$ to emerge, and was not considered in Maxey [1] or Tom and Bragg [11] where particle settling in an unbounded homogeneous flow was considered, for which the natural state that emerges is $\Phi < 0$.

C. Near wall region

As the particles approach the wall, gradients in the flow statistics become important and new mechanisms begin to control the particle settling velocity and concentration. In this case, all of the terms in (12) are in principle important.

The term R1 in (12) arises from the mean acceleration experienced by the particles due to gradients in their mean wall-normal velocity. This contribution vanishes for the zero-flux case $\Phi = 0$ but is finite in general for $\Phi \neq 0$. The second term on the right hand side, R2 in (12), describes a velocity arising from an inertially-based diffusive flux. For fluid particles, the turbulent motion of the flow provides a mechanism for macroscopic diffusive transport (this will be discussed in more detail below). For particles with inertia, their velocity is partially decoupled from the local fluid velocity, and this decoupling introduces a second source of diffusion that is captured by $\tau_p S \nabla_z \varrho$. For $St \gg 1$, the PDF equation reduces to a Fokker-Planck equation and in this regime $\tau_p S \nabla_z \varrho$ is the sole source of diffusion [26].

The third term, R3 in (12), describes the turbophoretic drift velocity [14]. Physically, this drift velocity may be understood as follows: suppose the particles are moving in a region of the boundary layer where $\nabla_z \langle uu \rangle > 0$. In this region, if the particle is moving towards the wall, then because they have come from regions where the flow has more TKE and because their response time is finite, they will be moving with greater kinetic energy than the local flow. On the other hand, if the particle is moving away from the wall then because they have come from regions where the flow has less TKE, they will be moving with less kinetic energy than the local flow. As a result, there is a symmetry breaking effect and the particles experience a velocity contribution towards the wall in regions where $\nabla_z \langle uu \rangle > 0$, and the opposite in regions where $\nabla_z \langle uu \rangle < 0$. In the limit $St \to 0$, the particle motion is governed only by the local flow, and so in this limit the turbophoretic effect vanishes. It also vanishes for $St \gg 1$ where the particles move ballistically through the boundary layer.

The fourth term, R4 in (12), describes a source of momentum arising from preferential sampling of the local flow. In the previous section, this contribution was considered in the homogeneous region of the flow. In that region, $\langle u^p(t) \rangle_z$ can only be finite if Sv is finite. Near the wall, however,

$\langle u^p(t)\rangle_z$ can be finite even if $Sv = 0$. This may be conceptually understood as follows. Suppose that due to the turbophoretic drift velocity and gravitational settling, the particles start to drift towards the wall, and their concentration builds up. If $\Phi = 0$, the particles must necessarily escape the near wall region, and so they must preferentially sample regions of the flow where $u^p(t) > 0$, leading to $\langle u^p(t)\rangle_z > 0$. When gravity is also present, $\langle u^p(t)\rangle_z$ may be also affected by the preferential sweeping mechanism, however, this is likely to be a sub-leading effect unless $\Phi < 0$, since if $\Phi = 0$ we must have $\langle u^p(t)\rangle_z > 0$ as discussed above (one exception is that for $St \gg 1$, $\tau_p S \nabla_z \varrho$ is significant and provides a mechanism to remove particles from the wall, such that $\langle u^p(t)\rangle_z > 0$ may not be required in order for particles to be able to escape the near-wall region; however, this is irrelevant since for $St \gg 1$, $\langle u^p(t)\rangle_z = 0$). As for the homogeneous region, $\langle u^p(t)\rangle_z = 0$ for $St \to 0$ and $St \to \infty$, the former because fluid particles uniformly sample the flow, and the latter because for $St \to \infty$ the particle motion is uncorrelated with the local fluid velocity.

Finally, the fifth (R5) and sixth (R6) terms on the rhs of (12) describe the Stokes settling velocity, and the artificial diffusion induced velocity, respectively.

D. Average fluid velocity seen by the particles

The average fluid velocity seen by the particles, $\langle u^p(t)\rangle_z$, plays in general an important role in determining the particle concentration and average vertical velocity. As noted earlier, the Rouse model for ϱ effectively amounts to assuming an eddy viscosity, gradient-diffusion closure for this term. Here we consider this in more detail.

Analytical theories show that $\varrho\langle u^p(t)\rangle_z$ has the form [23, 24, 51]

$$\varrho\langle u^p(t)\rangle_z = \zeta\varrho - \sum_{n=1}^{\infty} \mathcal{D}^{[n]}\nabla_z^n\varrho, \tag{19}$$

where ζ is a drift coefficient, and $\mathcal{D}^{[n]}$ are diffusion coefficients that depend on St, Sv and z in general. The precise form of these coefficients is not quoted here since they depend upon the particular analytical theory used (see, e.g. [25] for a detailed examination of the differences), and these details are not important for our discussion. In practice, in order to truncate this infinite expansion, most PDF based models of particle transport in turbulence assume that u has Gaussian statistics, for which the series reduces exactly to [24, 25, 51]

$$\varrho\langle u^p(t)\rangle_z = \zeta\varrho - \mathcal{D}^{[1]}\nabla_z\varrho. \tag{20}$$

Most interestingly, however, the asymptotic analysis of [52] showed that for a wall-bounded flow, the regime $z^+ \ll 1$ leads to $\sum_{n=1}^{\infty} \mathcal{D}^{[n]}\nabla_z^n\varrho \sim \mathcal{D}^{[1]}\nabla_z\varrho$ (where + denotes that the variable has been

11

normalized using wall units, in this case the friction length scale $\delta_\nu \equiv \sqrt{\nu/u_\tau}$, where u_τ is the wall friction velocity and ν is the fluid kinematic viscosity). This means that the contribution of the higher-order cumulants described by $\mathcal{D}^{[n]}$ for $n \geq 2$, which are neglected in (20) due to the Gaussian assumption, make a negligible contribution close to the wall. This is significant since it implies that (20) is accurate close to the wall, where the particle accumulation is strong and modeling is challenging. We also note that, as discussed in [25], models such as [53] incorrectly set $\zeta = 0$, which as we will soon see, has significant implications for modeling settling particles.

The fundamental difference between the drift $\zeta\varrho$ and diffusion $\mathcal{D}^{[1]}\nabla_z\varrho$ contributions in (20) is that whereas the diffusion contribution is only finite if there are finite gradients in the *mean* particle distribution ϱ, the drift contribution may be finite even if $\nabla_z\varrho = 0$, provided that there are inhomogeneities in the *instantaneous* particle distribution and that those inhomogeneities are correlated with the local flow. For example, for fully-mixed fluid particles, the spatial distribution is uniform for all times, and so both the diffusion and drift contributions vanish, leading to $\varrho\langle u^p(t)\rangle_z = 0$ [25]. On the other hand, for settling inertial particles in a homogeneous flow, the diffusion contribution is zero, but the drift term is finite, capturing the preferential sweeping mechanism proposed by Maxey [1]. Furthermore, an implication of the analysis in [25], that was subsequently demonstrated numerically in [27], is that even in the absence of gravity, if the instantaneous distribution of the inertial particles in non-uniform, then ζ is also finite if the turbulence is inhomogeneous. Therefore, for setting inertial particles in wall-bounded turbulence, ζ may be finite both due to the preferential sweeping mechanism and also due to turbulence inhomogeneity — a behavior not possible in HIT.

Phenomenological models that close $\varrho\langle u^p(t)\rangle_z$ using a gradient-diffusion hypothesis (such as the Rouse model, and those discussed in [47] for dilute suspensions) do not account for the drift contribution $\zeta\varrho$. The significance of this omission is that such models cannot account for Maxey's preferential sweeping mechanism (unless they account for it by modifying the Stokes settling velocity in the model). Note that for inhomogeneous flows, it is still the drift contribution $\zeta\varrho$ that formally accounts for preferential sweeping, and not the diffusive contribution. Therefore, this omission of $\zeta\varrho$ in gradient-diffusion closures is important for inhomogeneous flows, as well as homogeneous flows.

III. DIRECT NUMERICAL SIMULATIONS

A. Equations of motion

In order to explore the role of each term appearing in (11) and (12) and evaluate their respective contributions to the vertical velocities and distributions of the inertial particles, we use data from point-particle DNS of settling inertial particles in a horizontal, fully developed, incompressible turbulent open channel flow. This idealized framework allows us to compare directly to the theory described above. The DNS solves the incompressible Navier-Stokes equations

$$\partial_t \boldsymbol{U} + (\boldsymbol{U} \cdot \boldsymbol{\nabla}_{\boldsymbol{x}})\boldsymbol{U} = -\frac{1}{\rho_f}\boldsymbol{\nabla}_{\boldsymbol{x}}p + \nu\boldsymbol{\nabla}_{\boldsymbol{x}}^2\boldsymbol{U}, \tag{21}$$

where $\boldsymbol{U}(\boldsymbol{x},t)$ is the fluid velocity, $p(\boldsymbol{x},t)$ is the pressure (modified to include the hydrostatic contribution [54]), ν is the fluid kinematic viscosity, and ρ_f is the fluid density. A pseudospectral method is employed in the periodic directions (streamwise x and spanwise y), and second-order finite differences are used for spatial discretization in the wall-normal, z direction. The solution is advanced in time using a third-order Runge-Kutta (RK3) scheme. The incompressibility constraint $\boldsymbol{\nabla}_{\boldsymbol{x}} \cdot \boldsymbol{U} = 0$ is satisfied by prescribing the pressure via the solution of its Poisson equation $\boldsymbol{\nabla}_{\boldsymbol{x}}^2 p = \boldsymbol{\nabla}_{\boldsymbol{x}}\boldsymbol{U} : \boldsymbol{\nabla}_{\boldsymbol{x}}\boldsymbol{U}$.

The unladen flow field from DNS has been tested and validated by comparison with published data in multiple configurations; e.g., planar Couette flow at $Re_\tau = 40$ [55], wall-bounded channel flow at $Re_\tau = 227, 630$ [56], and open channel flow at $Re_\tau = 200, 550, 950$ [57]. On top of this flow, the trajectories of inertial particles are tracked via the standard point-particle approach by solving (1) and (2), and obtaining $\boldsymbol{U}^p(t)$ by interpolating to the particle position using a sixth-order Lagrange method. The particle Reynolds number appearing in Ψ is defined as $Re_p \equiv \|\boldsymbol{U}^p(t) - \boldsymbol{v}^p(t)\|d_p/\nu$, which is based on the magnitude of the particle slip velocity $\|\boldsymbol{U}^p(t) - \boldsymbol{v}^p(t)\|$ and the particle diameter d_p. In this work, the average Re_p is less than 1, which is far smaller than the suggested maximum $Re_p \approx 800$ for the Schiller-Naumann [43] model. As a result of the low Re_p, the correction to the Stokes drag is minimal in this study.

The primary purpose of this work is to develop a PDF approach for understanding settling and dispersion mechanisms in wall-bounded turbulence, and to evaluate the terms directly using the DNS framework. As such, we employ a simplified model system, which is limited to one-way coupling and a simple drag law (i.e. other terms, such as lift, history terms, etc. are neglected). While the basic point-particle technique used here is certainly subject to numerous simplifications and approximations, we consider it a prototypical testbed from which to analyze the theory described

13

(a) Free surface / vertical / spanwise / Particle laden flow / Wall / streamwise / Particle inlet/outlet

(b) Free surface / Particle inlet / vertical / spanwise / Particle laden flow / flux / Wall / streamwise / Particle outlet
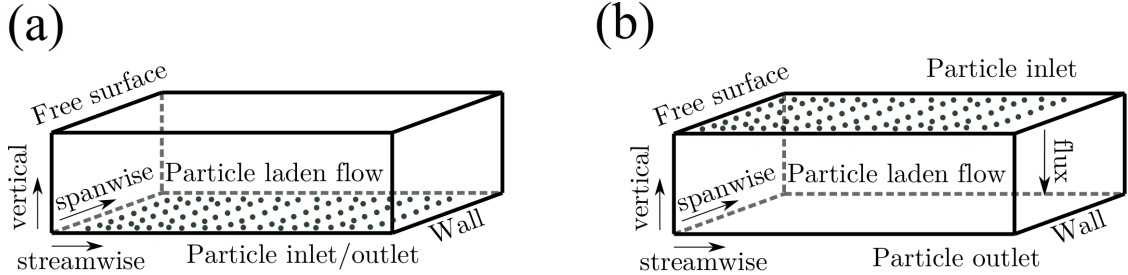
FIG. 1: (a) zero-flux configuration, in which a constant particle concentration is maintained using a reservoir just beneath the wall; (b) constant flux configuration, in which particles are initialized at the top of the domain and removed/replaced when they reach the wall.

in the previous sections. In this regard, in Wang *et al.* [56] our point-particle DNS code has been validated for inertial particles in the range $St^+ = 30 - 2000$ by comparisons against the code of Capecelatro and Desjardins [58], and compared with the experimental results of Fong *et al.* [21].

B. Boundary conditions and numerical parameters

We solve equation (21) at $Re_\tau \equiv u_\tau L_z / \nu = 315$, using a constant pressure gradient to force the flow. The domain size is $L_x \times L_y \times L_z = 2\pi \times 2\pi \times 1$ with a corresponding grid of $N_x \times N_y \times N_z = 128 \times 256 \times 128$. The grid is stretched in the wall-normal direction and thus the simulations have a resolution of $\Delta_x^+ \times \Delta_y^+ \times \Delta_z^+ = 15.4 \times 7.73 \times 0.5(wall), 4.49(center)$. The streamwise x and spanwise y directions are periodic, and the wall at $z = 0$ imposes a no-slip condition on the fluid velocity field. At the upper wall, $z = H$, a free-slip (i.e., zero-stress) condition is imposed on the fluid velocity. This setup provides a canonical case of wall-bounded turbulence, within which two distinct particle configurations are considered; figure 1 provides schematics of these two configurations which are guided by the theoretical development above.

In the first configuration, termed the "zero-flux" case (indicated by ZF), the particle boundary conditions are designed to maintain a statistically steady concentration within the domain and a mean net flux of zero ($\Phi = 0$) at all heights. At the upper domain boundary $z = H$, the particles rebound elastically, which is equivalent to a no-flux condition on the particle concentration. At the lower boundary, a Dirichlet condition for particle concentration is established, which in the Lagrangian framework is accomplished by maintaining a reservoir just beneath the wall at $z = 0$ whose concentration is kept constant.

14

In this setup, however, some mechanism is required for generating a flux of particles into the domain, so as to create a steady-state balance between gravitational settling and an upward emission flux. In physical applications, this emission mechanism would take the form of aerodynamic lift, dust/sand saltation, wave breaking, etc. Here, we generically account for this resuspension process by applying the weak Brownian diffusion term included in equation (1). We emphasize again that we do not intend to imply that inertial particles experience Brownian diffusion; rather, it is an artificial and simplified means of representing a wide variety of processes which in practice could release particles into the system. By setting $\kappa = \nu/100$, we limit the influence of this term only to the region immediately close to $z = 0$, and tests have confirmed that the diffusive contribution to the particle flux is negligible above the first Eulerian grid point. In the following sections, the diffusive contribution to equation (12) will be shown to be negligible as well. This zero-flux configuration is the same as that used in Richter and Chamecki [40].

In the second particle configuration, termed the "constant flux" case (denoted by CF and designed to provide $\Phi < 0$), the Lagrangian particles are instead placed at the upper boundary $(z = H)$ at a random location on the $x - y$ plane and given an initial vertical velocity equal to their terminal Stokes settling velocity $\tau_p g$ (the other two particle velocity components are set to zero). From here, the particles settle by gravity through the system and when they reach the lower boundary they are removed. This is somewhat similar to the recent experiments of Zheng *et al.* [59] who allow particles to settle through a turbulent boundary layer, although in the present simulations they are removed at the lower wall and two-way coupling is not considered. For each particle removed at the lower boundary, one is re-introduced at the upper boundary at a random location, and therefore the total number of particles N_p is exactly constant throughout the simulation (in contrast to the first no-flux configuration). After a sufficient time, the concentration profile and vertical flux attain statistical stationarity, with the non-zero net flux Φ independent of z and having magnitude that varies with τ_p. Note that for this constant-flux configuration, the diffusion term in (1) is not used (i.e., $\kappa = 0$), unlike the zero-flux configuration where it is required to enable particle suspension into the flow from the wall. Furthermore, periodic boundary conditions are applied to the particles in the horizontal directions of the flow for both the zero-flux and constant flux configurations.

These two simulation setups allow for contrasting the settling and dispersion mechanisms formulated in equation (12) when $\Phi = 0$ and when $\Phi \neq 0$. For each of the two configurations, six different simulations are performed, where the particle Stokes number is systematically increased. These are presented in table I, where case number 0 refers to the lowest Stokes number and 5 refers

to the highest. The particle diameter d_p^+ based on viscous wall units is 0.236 which is smaller than the grid cell size, in particular $d_p/\Delta_x \times d_p/\Delta_y \times d_p/\Delta_z = 0.015 \times 0.305 \times 0.472(wall), 0.053(center)$. We define two different Stokes numbers: St^+, which is based on viscous wall units and ranges between 0.003 and 46.5, and St_K, which is based on the vertically-averaged Kolmogorov timescale τ_K in the flow and ranges between 3.4×10^{-4} to 5.1. A Stokes number based on the local Kolmogorov timescale would decrease with increasing wall-normal position.

In order to isolate the effect of particle inertia on settling through wall-bounded turbulence, the gravitational acceleration g is varied with each case in order to maintain a constant settling parameter $Sv^+ \equiv \tau_p g/u_\tau = 2.5 \times 10^{-2}$, where u_τ is the friction velocity of the flow. This corresponds to $Sv_K \equiv \tau_p g/u_K = 7.4 \times 10^{-4}$ when the Stokes settling velocity is normalized by the vertically-averaged Kolmogorov velocity. Roughly speaking, this value of Sv^+ would correspond to a sand/dust grain with a diameter of $O(10~\mu\text{m})$ suspended over a windy surface (e.g. $u_\tau \approx O(0.1~\text{m/s})$). We choose this value since it was also used in Richter and Chamecki [40], allowing us to compare our results to theirs, and to further understand how the modified Rouse model that they considered, which was found to be accurate for $St \ll 1$, must be modified for predicting the case of general St. Moreover, since Sv^+ is fixed in our simulations by design, any observed changes in the particle statistics are solely due to changes in the Stokes number, not the settling number, and this aids in understanding the results. In the environment where g is constant, both St^+ and Sv^+ change as τ_p is varied, and this case will be considered in future work. As noted above, the flow Reynolds number is held fixed at $Re_\tau = 315$. While it would be instructive to test higher Reynolds numbers as well, especially in a range where so-called very-large-scale motions occur [60], we anticipate that most of the regimes and conclusions identified below would remain intact qualitatively, albeit with a narrowing of the extent near-wall, inhomogeneous region and an enlarging of the outer, quasi-homogeneous region.

IV. RESULTS & DISCUSSION

A. Behavior of average particle distribution and vertical velocity

In figure 2 we show results for the average total mass flux Φ, normalized vertical velocity $\langle w^p(t)\rangle_z/\tau_p g$, and spatial distribution ϱ for each of the cases, and for both the zero-flux (a,b,c) and constant-flux (d,e,f) configurations. We begin by describing the results for $\Phi, \langle w^p(t)\rangle_z, \varrho$, and will then turn to examine the underlying cause of their behavior in terms of the various mechanisms

16

TABLE I: Summary of the simulations. All cases are turbulent open channel flow at $Re_\tau = 315$. ZF refers to the "zero-flux" case while CF refers to the "constant flux" case. Case numbers $0 - 5$ indicate increasing Stokes numbers.

Case		d_p^+	St^+	St_K	Sv^+	Sv_K
ZF	CF					
0	0	0.236	0.003	3.4e-4	2.5×10^{-2}	7.4×10^{-4}
1	1	0.236	0.93	0.102	2.5×10^{-2}	7.4×10^{-4}
2	2	0.236	2.79	0.306	2.5×10^{-2}	7.4×10^{-4}
3	3	0.236	4.65	0.51	2.5×10^{-2}	7.4×10^{-4}
4	4	0.236	9.30	1.02	2.5×10^{-2}	7.4×10^{-4}
5	5	0.236	46.5	5.10	2.5×10^{-2}	7.4×10^{-4}

described by (11) and (12).

The results in figure 2 for Φ for the zero-flux case are computed using (11), and the small deviations of Φ from zero near the wall are due to statistical and numerical error when differentiating the DNS data for ϱ. For the zero-flux configuration, $\langle w^p(t) \rangle_z$ is zero away from the boundaries, but takes on finite values near the boundaries due to the contribution to the particle motion from the diffusive term involving κ in (1). As the wall is approached, ϱ begins to increase significantly, indicating that the particles accumulate near the wall.

For the constant-flux configuration, Φ varies non-monotonically with St^+, and is maximum for Case 4. As we will discuss momentarily, this non-monotonic behavior is due to turbulence since in the absence of turbulence, Φ would be independent of St^+ because Sv^+ is held constant in our DNS. Clearly, turbulence strongly influences this vertical mass flux, leading to enhancements of up to a factor of 4.5 for the cases considered. The average vertical velocity $\langle w^p(t) \rangle_z$ increases at all heights with increasing St^+, except in going from Case 4 to 5 where $\langle w^p(t) \rangle_z$ reduces with increasing St^+ in the upper portion of the domain. The results show that for Cases 1-3 as the particles move from the upper boundary towards the wall, they pass through a significant region where $\langle w^p(t) \rangle_z$ only slightly increases. As they get close to the wall, however, $\langle w^p(t) \rangle_z / \tau_p g$ suddenly drops due to the fluid velocity fluctuations reducing as the wall is approached. For Cases 4 and 5, $\langle w^p(t) \rangle_z$ varies significantly with z^+ throughout the entire domain, increasing significantly as z^+ is reduced down to $z^+ \approx 20$, below which $\langle w^p(t) \rangle_z$ reduces significantly. We note that for all cases, $\langle w^p(t) \rangle_z / \tau_p g$ drops as the wall is approached, but never actually reaches unity, despite the fact that the turbulent fluctuations vanish as $z^+ \to 0$.

It is important to emphasize that since $Sv^+ = 2.5 \times 10^{-2}$ in our DNS (fixed for all St^+), the actual settling velocities of the particles are very small compared with the velocity scales in the flow, i.e. $\langle w^p(t) \rangle_z \ll u_\tau \, \forall z^+$. Nevertheless, relative to $\tau_p g$, the enhancement to the particle settling velocity due to turbulence is significant, with $\langle w^p(t) \rangle_z / \tau_p g$ attaining values up to almost 10 (compared with previous results for homogeneous turbulence in either DNS where $\langle w^p(t) \rangle_z / \tau_p g \lesssim 2$ [49, 50] or experiments where $\langle w^p(t) \rangle_z / \tau_p g \lesssim 2.7$ [7]). Moreover, as explained in [61], the importance of gravitational settling on the particle motion in a wall-bounded flow is to be judged by comparing the Stokes settling velocity to the turbophoretic velocity, not comparing it to u_τ. This explains how we are able to observe a strong effect of gravity, even though Sv^+ is very small.

Concerning ϱ, for the constant-flux case we observe that away from the upper boundary, ϱ decreases slightly as z^+ decreases, until close to the wall where it sharply increases, indicating a near-wall accumulation of the particles. For this constant-flux case where there is no diffusion and (11) reduces to $\varrho = \Phi / \langle w^p(t) \rangle_z$, ϱ necessarily increases close to the wall if $\langle w^p(t) \rangle_z$ decreases as z^+ decreases, which we would expect if turbulence plays a role in the particle motion.
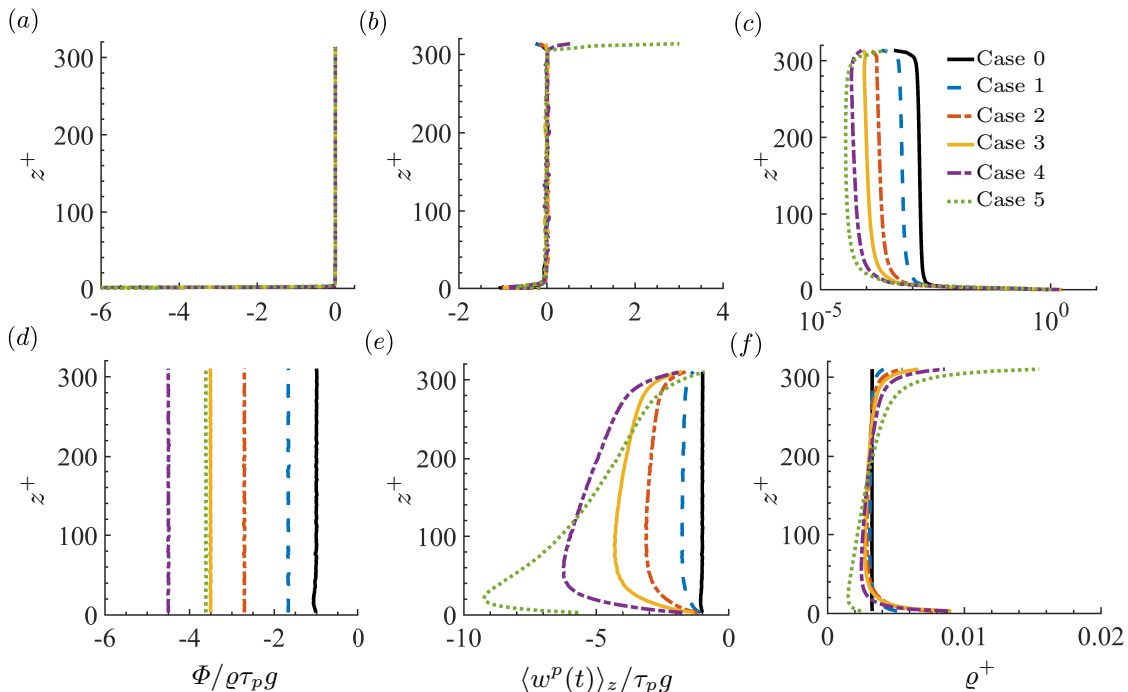

FIG. 2: DNS results for the total mass flux (a, d), normalized average vertical particle velocity (b, e), and spatial distribution (c, f). Different colors correspond to the different cases. Plots (a,b,c) and (d,e,f) correspond to the zero-flux and constant-flux cases, respectively.

In figure 3 we plot the results for ϱ in a log-log scale in order to examine the behavior close to the wall. For the zero-flux configuration, we find that for $z^+ \lesssim 6$, ϱ increases sharply, but not exactly as a power law. Moreover, our results indicate that even if one approximately fits the data with a power law, the exponent increases with increasing St^+, contrary to the behavior discussed in Sikovsky [52] and Johnson *et al.* [16]. This discrepancy may be due either to the inclusion of gravity or the molecular diffusion term used to re-suspend the particles from the wall, neither of which were considered in Sikovsky [52] or Johnson *et al.* [16]. For the constant flux configuration, the results in figure 3 show that for $z^+ \lesssim 20$, ϱ sharply increases, with a behavior that is again close to, but not exactly a power law.
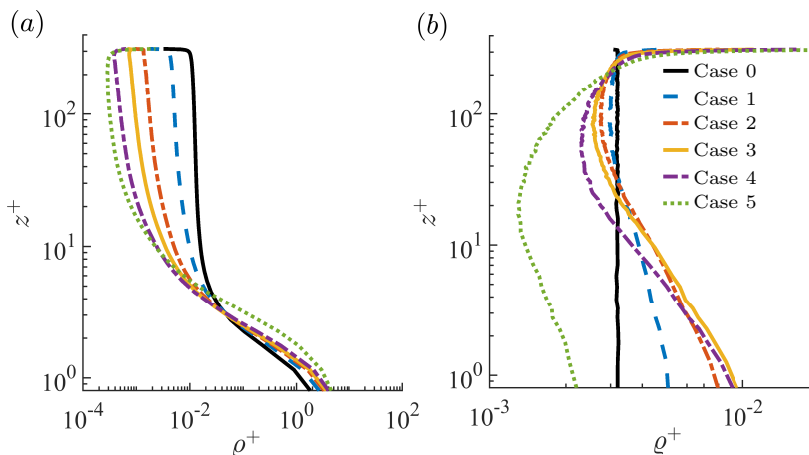
FIG. 3: Results for ϱ^+ plotted in a log-log scale to emphasize the behavior close to the wall. (a) zero-flux configuration, (b) constant flux configuration.

B. Mechanisms controlling the wall-normal particle motion

In order to understand the physical mechanisms governing the behavior of $\langle w^p(t) \rangle_z$ and ϱ, we compute the various terms that contribute to $\langle w^p(t) \rangle_z$ according to (12). Figure 4 shows the results for the zero-flux case. Throughout most of the domain where $\langle w^p(t) \rangle_z = 0$, we find that for Cases 0 and 1, $\langle w^p(t) \rangle_z \approx \langle u^p(t) \rangle_z - \tau_p g$, which is the behavior expected for a quasi-homogeneous flow according to (17). However, the results in figure 5 show that over this same region, the vertical fluid Reynolds stress $\langle uu \rangle$ varies appreciably. This may be understood by noting that in the limit $St^+ \to 0$, with Sv^+ finite, (17) also reduces to the result $\langle w^p(t) \rangle_z = \langle u^p(t) \rangle_z - \tau_p g$. For larger St^+, the inhomogeneity does play a role, and for Cases 2-5 $\langle w^p(t) \rangle_z \approx \langle u^p(t) \rangle_z - \tau_p g$ does not hold

because a significant contribution arises from the turbophoretic velocity $-\tau_p \nabla_z S$ in (12) (term R3). This turbophoretic velocity switches from being positive in the upper portion of the domain to negative in the lower portion due to the sign of $\nabla_z S$, whose sign changes because of the change of sign in the gradient of the fluid Reynolds stress (see figure 5). This means that in the upper portion of the domain, both the turbophoretic velocity and the velocity arising from preferential sampling of the fluid, i.e $\langle u^p(t) \rangle_z$, act against the Stokes settling velocity $-\tau_p g$ in order to preserve $\Phi = 0$. Close to the wall where $-\tau_p \nabla_z S$ changes sign and causes particles to drift towards the wall, $\langle u^p(t) \rangle_z$ increases in magnitude, and an inertial diffusion contribution from $(\tau_p/\varrho)S\nabla_z \varrho$ (term R2) is also activated that preserves $\Phi = 0$. This diffusion contribution becomes increasingly important as St is increased, as expected based on the discussion in §II C, and consistent with the results in [16]. For all cases, we find that the contribution from the acceleration $-(\tau_p/2)\nabla_z \langle w^p(t)\rangle_z^2$ (term R1) is negligible. Furthermore, the artificial diffusion $(\tau_p \kappa/\varrho)\nabla_z^2 \varrho \langle w^p(t) \rangle_z$ (term R6) term is indeed negligible as designed, even close to the wall, since its only purpose was to act as a mechanism for suspending particles from the lower boundary.
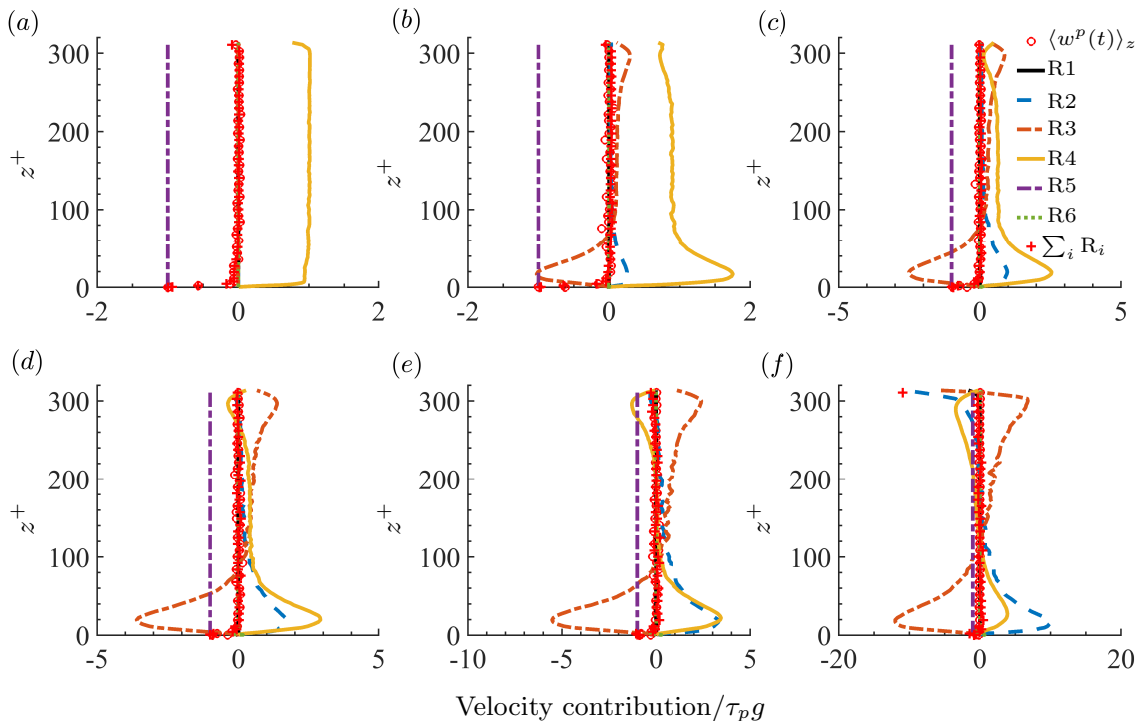

FIG. 4: Results for the averaged vertical particle velocity $\langle w^p(t)\rangle_z$, compared with the different contributions to this velocity according to (12), for the zero-flux configuration. Each subplot (a), (b), etc corresponds to Case 1, 2, etc, respectively, and R_i denotes the ith term on the rhs of (12).
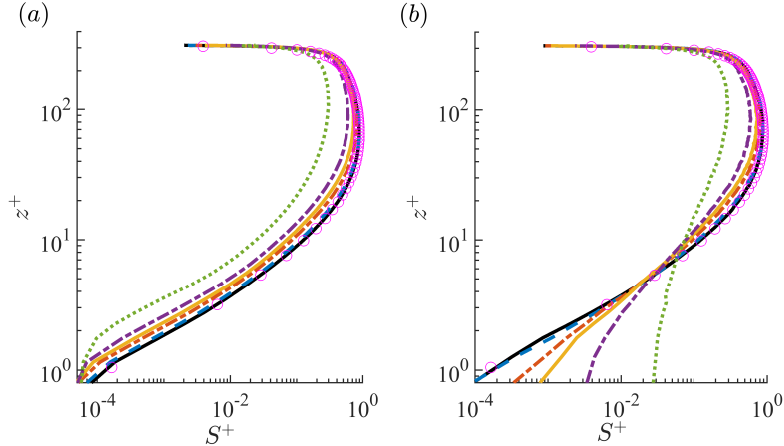
FIG. 5: Results for S^+ plotted in a log-log scale to emphasize the behavior close to the wall. (a) Zero-flux configuration, (b) constant flux configuration. Legend is the same as figure 2, except for ∘ which corresponds to the fluid wall-normal Reynolds stress $\langle u^+ u^+ \rangle$.

In figure 6 we similarly compute for the constant-flux configuration the various terms that contribute to $\langle w^p(t) \rangle_z$ according to (12). Unlike the zero-flux case, for the constant-flux case the particles have a finite average vertical settling velocity. For $St^+ \to 0$, $\langle w^p(t) \rangle_z / \tau_p g \to 1$, while for finite St^+, $\langle w^p(t) \rangle_z / \tau_p g$ attains values of up to 10, indicating remarkably strong enhancements of the average particle settling speeds due to the combined effects of turbulence and particle inertia (recall that $\langle w^p(t) \rangle_z / \tau_p g = 1 \, \forall St^+$ in the absence of turbulence). For $z^+ > O(100)$, the dominant cause of the enhanced settling velocity comes from $\langle u^p(t) \rangle_z$ (term R4). As discussed in §II B, when $\Phi < 0$ and the flow is homogeneous, $\langle u^p(t) \rangle_z$ is finite due to the preferential sweeping mechanism [1, 11]. However, as explained in §II D, for wall-bounded turbulence, there is an additional contribution to $\langle u^p(t) \rangle_z$ arising from the combined effects of particle inertia and turbulence inhomogeneity. This additional contribution may explain why we observe larger values for $\langle w^p(t) \rangle_z / \tau_p g$ at $z^+ > O(100)$ than have previously been observed for homogeneous turbulence in either DNS where $\langle w^p(t) \rangle_z / \tau_p g \lesssim 2$ [49, 50] or experiments where $\langle w^p(t) \rangle_z / \tau_p g \lesssim 2.7$ [7].

As the wall is approached, $\langle u^p(t) \rangle_z$ (term R4) begins to reduce in magnitude (since $u^p(t) \to 0$ for $z^p(t) \to 0$), while the turbophoretic velocity $-\tau_p \nabla_z S$ (term R3) suddenly grows in magnitude, and dominates $\langle w^p(t) \rangle_z$ close to the wall. It is the contribution from $-\tau_p \nabla_z S$ that enables $\langle w^p(t) \rangle_z$ to remain finite as the wall is approached. Physically, the inertial particle remembers its interaction with the turbulence along its path-history in regions where the TKE is finite, and this enables $w^p(t)$ to be finite even if $u^p(t) = 0$, such as at the wall. It is this path-history effect that is described by

21

$-\tau_p \nabla_z S$, as explained in §II C. These results therefore show that as the wall is approached, the importance of the preferential sweeping mechanism in determining the particle settling velocity gives way to the turbophoretic drift mechanism.

Comparing figure 4 with figure 6, we see that in both cases, near the wall the dominant negative contribution to $\langle w^p(t) \rangle_z$ comes from the turbophoretic drift (unless St^+ is very small), and that $-\tau_p \nabla_z S$ attains a peak magnitude near the wall that is similar for both cases. The main difference between the two cases concerns the behavior of the positive contributions to $\langle w^p(t) \rangle_z$. In particular, for the constant-flux configuration, the absorbing wall boundary condition means that once the particles have reached the wall, they do not have enough time close to the wall in order to experience sufficiently large positive values of $u^p(t)$ that can transport them away from the wall. This differs from the zero-flux case for which $\langle u^p(t) \rangle_z > 0$ near the wall enabling the particles to be suspended back into the flow from the near wall region, producing the zero-flux state. The inertial-diffusion term $-\tau_p S \nabla_z \varrho$ (term R2) is also much smaller in the near wall region for the constant flux case than it is for the zero-flux case.

Similar to the zero-flux configuration, for the constant-flux configuration we find that the contribution from the acceleration $-(\tau_p/2) \nabla_z \langle w^p(t) \rangle_z^2$ is negligible, even close to the wall. Therefore, for both configurations, the first and sixth terms on the rhs of (12), R1 and R6, may be safely neglected (R6 is identically zero for our constant flux case).
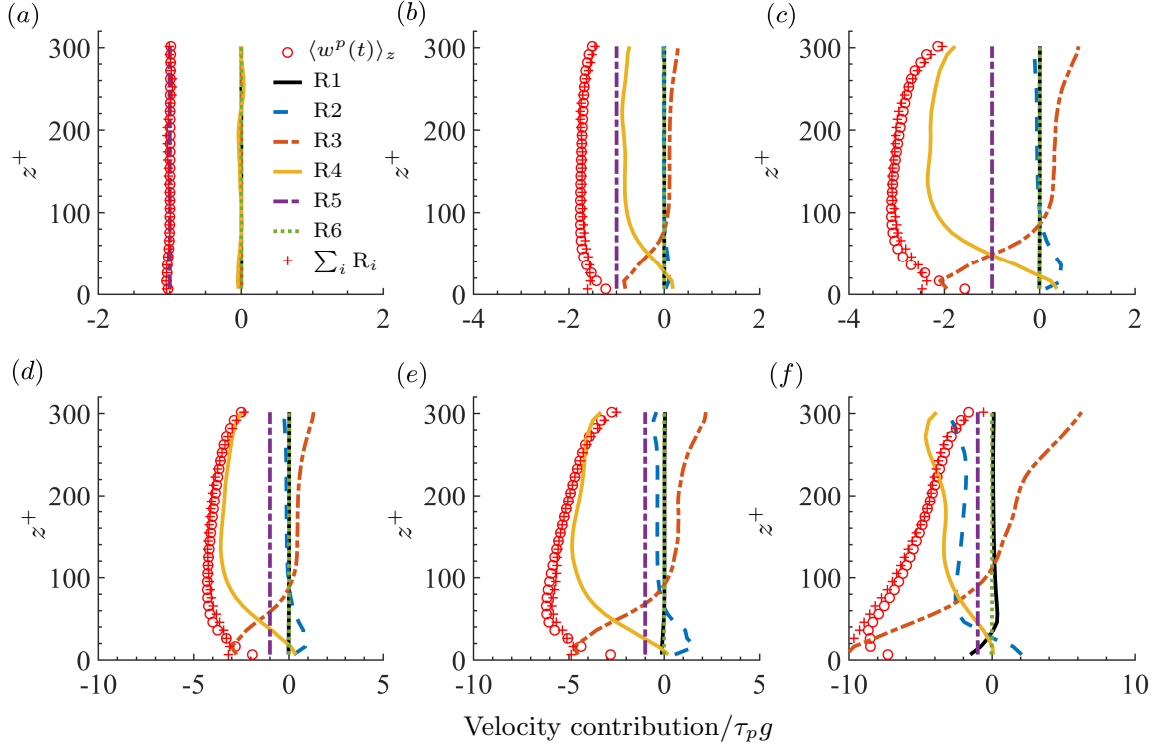
FIG. 6: Results for the averaged vertical particle velocity $\langle w^p(t)\rangle_z$, compared with the different contributions to this velocity according to (12), for the constant flux configuration. Each subplot (a), (b), etc corresponds to Case 1, 2, etc, respectively, and R_i denotes the ith term on the rhs of (12).

C. Extending the Rouse model

As stated in the introduction, one of the motivations for our study is to consider how the Rouse model for particle concentration (that was derived for $St^+ \to 0$, with finite St^+/Fr^+) must be extended in order to apply for $St^+ \geq O(1)$. Based on the results in this section, terms R1 and R6 in (12) may be neglected. Furthermore, if we use (20) to model $\langle u^p(t)\rangle_z$, then for the zero-flux case we obtain the approximate version of (12)

$$0 \approx -(\tau_p S + \mathcal{D}^{[1]} + \kappa)\nabla_z \varrho - \varrho\Big(\tau_p \nabla_z S - \zeta + \tau_p g\Big). \tag{22}$$

Comparing this with the Rouse model in (16) reveals a number of differences, and points to the way in which the Rouse model is to be extended to apply for $St^+ \geq O(1)$. First, Rouse's eddy-diffusion model $\mathcal{K}$ that only applies in the log-law region can be replaced with the more general diffusion coefficient $\mathcal{D}^{[1]}$ that is valid for arbitrary z^+, and for which a simple closed expression is given in Zaichik [53]. Second, an additional contribution to the diffusion coefficient must be accounted for,

23

namely $\tau_p S$, which captures the diffusion contribution arising because of the imperfect coupling between the fluid and inertial particle velocities. Third, the turbophoretic velocity $-\tau_p \nabla_z S$ must be accounted for. Fourth, the drift contribution ζ must be accounted for that captures the effects of the preferential sweeping mechanism of [1], as well as preferential sampling of the flow due to turbulence inhomogeneity. The study of [40] captures some of these additional effects for $St^+ \ll 1$, but does not apply for $St^+ \geq O(1)$.

The terms involving S are unclosed, and S must be predicted, yet its transport equation is unclosed. Models such as [53] attempt to close these transport equations using a quasi-normal approximation. While this may lead to reasonable results far enough away from the wall, near the wall (e.g. $z^+ \leq O(10)$) such a closure is known to yield behavior that is inconsistent with the behavior predicted using asymptotic analysis (see [52]). Developing closures that are consistent with this asymptotic behavior is crucial since it is in the near wall region where most of the complexity in the particle motion occurs, e.g. where the strong particle accumulation occurs. It is also necessary to test the accuracy of the closure in equation (20), and to develop a closed form expression for the drift velocity ζ. These issues are extremely important in achieving accurate representations of particle transport in coarse-scale models, including in both LES and RANS-based schemes. In the context of wall-modeled LES, which was the motivation behind the work of Johnson *et al.* [16], an accurate subgrid treatment of near-wall behavior could ultimately be described by appropriate closures. At even coarser scales, such as the representation of the atmospheric surface layer in dust-laden numerical weather prediction models, flux-profile relationships are required to provide lower boundary conditions to fields of conserved scalars — what to do when these scalars both settle and experience inertia remains unknown, and in practice the standard Rouse model is used even in these situations. Consideration of these issues will be the subject of our future work.

V. CONCLUSIONS

We have used a combination of theoretical analysis and point-particle DNS data to explore the mechanisms and behavior of the settling velocities and spatial distributions of small inertial particles in a wall-bounded turbulent flow. Two different flow configurations were considered, one where the particle mass flux is zero, and the other where it is constant and negative.

The theory is based on the exact transport equations for the particle statistics that are derived from a phase-space, master PDF equation. This allowed us to identify and consider the specific contribution to the particle settling velocities and spatial distribution coming from distinct physical

mechanisms in the system, which we could then explore using our DNS data.

For the zero-flux case, the DNS results revealed that the vertical particle motion is similar to the behavior without gravitational settling. For the constant flux case, the combined effects of turbulence and particle inertia lead to average vertical particle velocities that can significantly exceed the Stokes settling velocity, similar to what is seen in HIT. In particular, as the particles approach the wall, their average vertical velocity can significantly increase, depending on St^+, reaching values up to ten times the Stokes settling velocity. Below a certain z^+, however, the average vertical particle velocities reduce due to the reduction of the fluid velocities as the wall is approached.

Concerning the mechanisms governing the average vertical particle velocity, in the zero-flux case, at heights $z^+ \geq O(100)$, the average velocity is zero, and for the lower St^+ cases this is due to a downward contribution from the Stokes settling velocity that is precisely balanced by an upward velocity arising from the particles preferentially sampling regions of the flow where the fluid velocity is positive. For larger St^+ there is also an upward turbophoretic velocity (since in this region the fluid Reynolds stresses decay with increasing z^+) that acts together with the preferential sampling effect to counter balance the Stokes settling velocity. As the particles approach the wall, they experience a strong turbophoretic velocity contribution that drives them towards the wall, that is counteracted by an upward velocity contribution arising from the preferential sampling of regions where the fluid velocity is positive, and additional contributions arising from diffusive mechanisms that are driven by gradients in the concentration field.

For the constant flux case, for $z^+ \geq O(100)$ the average vertical particle velocities can significantly exceed the Stokes settling velocity due to the particles preferentially sampling regions where the fluid velocity is negative. This effect is associated with the preferential sweeping mechanism of [1]. As St^+ increases, there is also an upward contribution from the turbophoretic velocity, but this is overwhelmed by the contribution from preferential sweeping. As the particles approach the wall, the contribution to the average vertical particle velocity coming from the preferential sweeping mechanism becomes small, and a downward contribution from the turbophoretic velocity dominates the behavior.

For future work, it is important to consider how the behavior observed here changes when Sv^+ is varied, since this quantity was held fixed in our simulations in order to isolate the effect of St^+. In the environment, St^+ and Sv^+ will vary simultaneously, and as such, different mechanisms may compete and play dominant roles compared with the case we have explored. It will also be interesting to perform DNS using more particles, and/or longer simulation times in order to

generate robust statistics very close to the wall so that the asymptotic behavior there may be explored in detail. Finally, one of the motivations for this study was to better understand the role of particle inertia in order to understand how the Rouse model for the particle concentration, which was derived for $St^+ \to 0$ (with finite St^+/Fr^+), can be modified for $St^+ \geq O(1)$. Our study, and results from the future research just discussed can provide crucial insights guiding the particular terms and mechanisms that must be incorporated into such an extended Rouse model. For example, our present results show that in order for the Rouse model to describe the regime $St^+ \geq O(1)$, it must be extended to include the turbophoretic drift velocity, a diffusion mechanism associated with the inertial particle velocities being partially de-coupled from the local fluid velocity, as well as the term describing the preferential sampling of the fluid velocity field, which captures the preferential sweeping mechanism.

ACKNOWLEDGEMENTS

---

[1] M. Maxey, The gravitational settling of aerosol particles in homogeneous turbulence and random flow fields, J. Fluid Mech. **174**, 441 (1987).

[2] L.-P. Wangand M. R. Maxey, Settling velocity and concentration distribution of heavy particles in homogeneous isotropic turbulence, J. Fluid Mech. **256**, 27 (1993).

[3] C. Y. Yangand U. Lei, The role of the turbulent scales in the settling velocity of heavy particles in homogeneous isotropic turbulence, J. Fluid Mech. **371**, 179 (1998).

[4] A. Aliseda, A. Cartellier, F. Hainaux, and J. C. Lasheras, Effect of preferential concentration on the settling velocity of heavy particles in homogeneous isotropic turbulence, J. Fluid Mech. **468**, 77 (2002).

[5] T. S. Yangand S. S. Shy, The settling velocity of heavy particles in an aqueous near-isotropic turbulence, Phys. Fluids **15**, 868 (2003).

[6] T. S. Yangand S. S. Shy, Two-way interaction between solid particles and homogeneous air turbulence: Particle settling rate and turbulence modification measurements, J. Fluid Mech. **526**, 171 (2005).

[7] A. J. Petersen, L. Baker, and F. Coletti, Experimental study of inertial particles clustering and settling

in homogeneous turbulence, J. Fluid Mech. **864**, 925-970 (2019).

[8] A. Nemes, T. Dasari, J. Hong, M. Guala, and F. Coletti, Snowflakes in the atmospheric surface layer: observation of particle–turbulence dynamics, J. Fluid Mech. **814**, 592 (2017).

[9] B. Rosa, H. Parishani, O. Ayala, and L.-P. Wang, Settling velocity of small inertial particles in homogeneous isotropic turbulence from high-resolution dns, Int. J. Multiphase Flow **83**, 217 (2016).

[10] G. H. Good, P. J. Ireland, G. P. Bewley, E. Bodenschatz, L. R. Collins, and Z. Warhaft, Settling regimes of inertial particles in isotropic turbulence, J. Fluid Mech. **759**, 10.1017/jfm.2014.602 (2014).

[11] J. Tomand A. D. Bragg, Multiscale preferential sweeping of particles settling in turbulence, J. Fluid Mech. **871**, 244?270 (2019).

[12] C. Marchioliand A. Soldati, Mechanisms for particle transfer and segregation in a turbulent boundary layer, J. Fluid Mech. **468**, 283 (2002).

[13] D. H. Richterand P. P. Sullivan, Modification of near-wall coherent structures by inertial particles, Phys. Fluids **26**, 103304 (2014).

[14] M. Reeks, The transport of discrete particles in inhomogeneous turbulence, J. Aerosol Sci. **14**, 729 (1983).

[15] G. Sardina, P. Schlatter, L. Brandt, F. Picano, and C. M. Casciola, Wall accumulation and spatial localization in particle-laden wall flows, J. Fluid Mech. **699**, 50 (2012).

[16] P. L. Johnson, M. Bassenne, and P. Moin, Turbophoresis of small inertial particles: theoretical considerations and application to wall-modelled large-eddy simulations, J. Fluid Mech. **883**, A27 (2020).

[17] M. Righettiand G. P. Romano, Particle-fluid interactions in a plane near-wall turbulent flow, J. Fluid Mech. **505**, 93 (2004).

[18] K. T. Kigerand C. Pan, Suspension and turbulence modification effects of solid particulates on a horizontal turbulent channel flow, J. Turbul. **3**, N19 (2002).

[19] J. Li, H. Wang, Z. Liu, S. Chen, and C. Zheng, An experimental study on turbulence modification in the near-wall boundary layer of a dilute gas-particle channel flow, Exp. Fluids **53**, 1385 (2012).

[20] J. D. Kulick, J. R. Fessler, and J. K. Eaton, Particle response and turbulence modification in fully developed channel flow, J. Fluid Mech. **277**, 109 (1994).

[21] K. O. Fong, O. Amili, and F. Coletti, Velocity and spatial distribution of inertial particles in a turbulent channel flow, J. Fluid Mech. **872**, 367 (2019).

[22] J. Leeand C. Lee, The effect of wall-normal gravity on particle-laden near-wall turbulence, J. Fluid Mech. **873**, 475 (2019).

[23] M. W. Reeks, On a kinetic equation for the transport of particles in turbulent flows, Phys. Fluids **3**, 446 (1991).

[24] D. Swailesand K. Darbyshire, A generalized Fokker-Planck equation for particle transport in random media, Physica A **242**, 38 (1997).

[25] A. Bragg, D. C. Swailes, and R. Skartlien, Drift-free kinetic equations for turbulent dispersion, Phys. Rev. E **86**, 056306 (2012).

[26] A. Braggand L. Collins, New insights from comparing statistical theories for inertial particles in turbulence: I. spatial distribution of particles., New J. Phys. **16**, 055013 (2014).

[27] A. Bragg, D. C. Swailes, and R. Skartlien, Particle transport in a turbulent boundary layer: Non-local closures for particle dispersion tensors accounting for particle-wall interactions, Phys. Fluids **24**, 103304 (2012).

[28] H. Rouse, Modern conceptions of the mechanics of turbulence, Trans. Am. Soc. Civ. Eng. **102**, 463 (1937).

[29] R. Sommerfeldand J. A. Businger, The density profile of blown snow, J. Geophys. Res. **70**, 3303 (1965).

[30] W. A. Hoppel, G. M. Frick, and J. W. Fitzgerald, Surface source function for sea-salt aerosol and aerosol dry deposition to the ocean surface, J. Geophys. Res. **107**, 1 (2002).

[31] E. R. Lewisand S. E. Schwartz, *Sea Salt Aerosol Production: Mechanisms, Methods, Measurements, and Models - a Critical Review* (American Geophysical Union, 2004) p. 413.

[32] M. Chamecki, C. Meneveau, and M. B. Parlange, Large eddy simulation of pollen transport in the atmospheric boundary layer, J. Aerosol Sci. **40**, 241 (2009).

[33] R. Kind, One-dimensional aeolian suspension above beds of loose particles - a new concentration-profile equation, Atmospheric Environment. Part A. General Topics **26**, 927 (1992).

[34] L. Freire, M. Chamecki, and J. Gillies, Flux-profile relationship for dust concentration in the stratified atmospheric surface layer, Boundary Layer Meteorol. **160**, 249 (2016).

[35] I. D. Nissanka, H. J. Park, L. S. Freire, M. Chamecki, J. S. Reid, and D. H. Richter, Parameterized vertical concentration profiles for aerosols in the marine atmospheric boundary layer, J. Geophys. Res. Atmos. **123**, 9688 (2018).

[36] Y. Pan, M. Chamecki, and S. A. Isard, Dispersion of heavy particles emitted from area sources in the unstable atmospheric boundary layer, Boundary Layer Meteorol. **146**, 235 (2013).

[37] Z. Zhu, R. Hu, X. Zheng, and Y. Wang, On dust concentration profile above an area source in a neutral atmospheric surface layer, Environ. Fluid Mech. **17**, 1171 (2017).

[38] T. Berkand F. Coletti, Transport of inertial particles in high-Reynolds-number turbulent boundary layers, Journal of Fluid Mechanics **903**, A18 (2020).

[39] L. J. Bakerand F. Coletti, Particle-fluid-wall interaction of inertial spherical particles in a turbulent boundary layer, Journal of Fluid Mechanics **934**, A39 (2021).

[40] D. H. Richterand M. Chamecki, Inertial effects on the vertical transport of suspended particles in a turbulent boundary layer, Boundary Layer Meteorol. **167**, 235 (2018).

[41] O. Druzhinin, On the two-way interaction in two-dimensional particle-laden flows: the accumulation of particles and flow modification, J. Fluid Mech. **297**, 49 (1995).

[42] J. Ferryand S. Balachandar, A fast eulerian method for disperse two-phase flow, Int. J. Multiphase Flow **27**, 1199 (2001).

[43] V. Schiller, ber die grundlegenden berechnungen bei der schwerkraftaufbereitung, Z. Vereines Deutscher Inge. **77**, 318 (1933).

[44] J. B. McLaughlin, The lift on a small sphere in wall-bounded linear shear flows, Journal of Fluid Mechanics **246**, 249 (1993).

[45] A. D. Bragg, P. J. Ireland, and L. R. Collins, On the relationship between the non-local clustering mechanism and preferential concentration, J. Fluid Mech. **780**, 327 (2015).

[46] V. Garzó, S. Tenneti, S. Subramaniam, and C. Hrenya, Enskog kinetic theory for monodisperse gas–solid flows, Journal of Fluid Mechanics **712**, 129 (2012).

[47] R. O. Fox, On multiphase turbulence models for collisional fluid-particle flows, Journal of Fluid Mechanics **742**, 368 (2014).

[48] J. Capecelatro, O. Desjardins, and R. O. Fox, Strongly coupled fluid-particle flows in vertical channels. i. reynolds-averaged two-phase turbulence statistics, Physics of Fluids **28**, 033306 (2016).

[49] J. Bec, H. Homann, and S. S. Ray, Gravity-driven enhancement of heavy particle clustering in turbulent flow, Phys. Rev. Lett. **112**, 184501 (2014).

[50] P. J. Ireland, A. D. Bragg, and L. R. Collins, The effect of reynolds number on inertial particle dynamics in isotropic turbulence. part 2. simulations with gravitational effects, J. Fluid Mech. **796**, 659 (2016).

[51] M. W. Reeks, Particle drift in turbulent flows: the influence of local structure and inhomogeneity (2012), arXiv:1205.2731 [physics.flu-dyn].

[52] D. P. Sikovsky, Singularity of inertial particle concentration in the viscous sublayer of wall-bounded turbulent flows, Flow, Turbulence and Combustion **92** (2014).

[53] L. I. Zaichik, A statistical model of particle transport and heat transfer in turbulent shear flows, Phys. Fluids **11**, 1521 (1999).

[54] S. B. Pope, *Turbulent Flows* (Cambridge University Press, New York, 2000).

[55] G. Wangand D. H. Richter, Modulation of the turbulence regeneration cycle by inertial particles in planar couette flow, J. Fluid Mech. **861**, 901 (2019).

[56] G. Wang, K. O. Fong, F. Coletti, J. Capecelatro, and D. H. Richter, Inertial particle velocity and distribution in vertical turbulent channel flow: a numerical and experimental comparison, Int. J. Multiphase Flow , 103105 (2019).

[57] G. Wangand D. H. Richter, Two mechanisms of modulation of very-large-scale motions by inertial particles in open channel flow, J. Fluid Mech. **868**, 538-559 (2019).

[58] J. Capecelatroand O. Desjardins, An Euler–Lagrange strategy for simulating particle-laden flows, J. Comput. Phys. **238**, 1 (2013).

[59] X. Zheng, G. Wang, and W. Zhu, Experimental study on the effects of particle-wall interactions on VLSM in sand-laden flows, J. of Fluid Mech. **914**, A35 (2021).

[60] N. Hutchinsand I. Marusic, Evidence of very long meandering features in the logarithmic region of turbulent boundary layers, Journal of Fluid Mechanics **579**, 1 (2007).

[61] A. D. Bragg, D. H. Richter, and G. Wang, When is settling important for particle concentrations in wall-bounded turbulent flows? (2021), arXiv:2101.04607 [physics.flu-dyn].